HHS Public Access

Author manuscript

Cell Rep. Author manuscript; available in PMC 2017 June 16.

Published in final edited form as:

Cell Rep. 2017 April 18; 19(3): 532–544. doi:10.1016/j.celrep.2017.03.068.

Loss of Navβ4-mediated regulation of sodium currents in adult Purkinje neurons disrupts firing and impairs motor coordination and balance

Joseph L. Ransdell[1], **Edward Dranoff**[1], **Brandon Lau**[1], **Wan-Lin Lo**[2], **David L. Donermeyer**[2], **Paul M. Allen**[2], and **Jeanne M. Nerbonne**[1,*]

[1]Departments of Developmental Biology and Internal Medicine, Washington University School of Medicine, St. Louis, MO 63110, USA

[2]Department of Pathology and Immunology, Washington University School of Medicine, St. Louis, MO 63110, USA

SUMMARY

The resurgent component of voltage-gated Na^+ (Nav) currents, I_{NaR}, has been suggested to provide the depolarizing drive for high frequency firing and to be generated by voltage-dependent Nav channel block (at depolarized potentials) and unblock (at hyperpolarized potentials) by the accessory Navβ4 subunit. To test these hypotheses, we examined the effects of the targeted deletion of *Scn4b* (Navβ4) on I_{NaR} and on repetitive firing in cerebellar Purkinje neurons. We show here that *Scn4b*$^{-/-}$ animals have deficits in motor coordination and balance and that firing rates in *Scn4b*$^{-/-}$ Purkinje neurons are markedly attenuated. Acute, *in vivo* shRNA-mediated "knockdown" of Navβ4 in adult Purkinje neurons also reduced spontaneous and evoked firing rates. Dynamic clamp-mediated addition of I_{NaR} partially rescued firing in *Scn4b*$^{-/-}$ Purkinje neurons. Voltage-clamp experiments revealed that I_{NaR} was reduced (by ~50%), but not eliminated, in *Scn4b*$^{-/-}$ Purkinje neurons, revealing that additional mechanisms contribute to generation of I_{NaR}.

Graphical abstract

*To whom correspondence should be addressed at: Jeanne M. Nerbonne, Department of Internal Medicine, Washington University School of Medicine, 660 South Euclid Avenue, St. Louis, MO 63110, Tel: (314) 362-2564, jnerbonne@wustl.edu.
Lead Contact: Jeanne M. Nerbonne

AUTHOR CONTRIBUTIONS

J.L.R. performed viral injections, behavioral and electrophysiological experiments. E.D. developed the I_{NaR} model used in the dynamic clamp experiments and B.L. performed behavioral experiments. W-L.L, D.L.D. and P.M.A. generated, validated and characterized the *Scn4b*$^{-/-}$ mouse line. J.L.R. and J.M.N. designed the experiments and analyzed the data. J.L.R., J.M.N and P.M.A. wrote the manuscript.

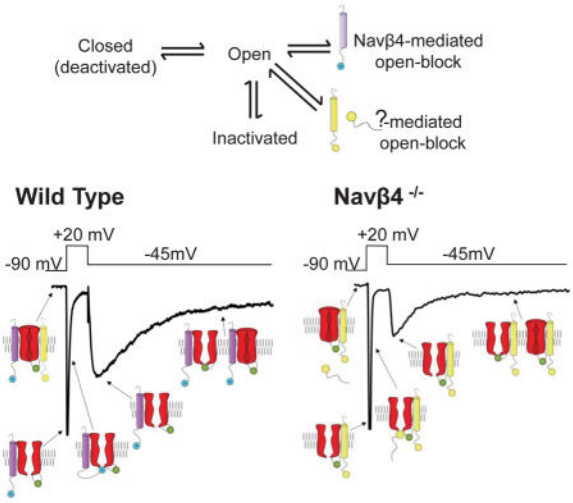

Keywords

cerebellum; resurgent sodium current; *Scn4b*$^{-/-}$; *Scn4b*-targeted shRNA; dynamic clamp

INTRODUCTION

Purkinje neurons function as the sole output of the cerebellar cortex, firing repetitively to provide tonic inhibition to the deep cerebellar nuclei (Billard et al., 1993; Gauck and Jaeger, 2000). To fire at high frequencies (~100Hz), Purkinje neurons express a unique suite of voltage-dependent currents (Raman and Bean, 1999a; Sacco and Tempia, 2002; Khaliq et al., 2003). Previous work has identified critical roles for voltage-dependent Na^+ (Nav) currents, encoded by the Nav1.1 (*Scn1a*), Nav1.2 (*Scn2a*) and Nav1.6 (*Scn8a*) pore-forming (α) subunits, in the regulation of Purkinje neuron excitability and cerebellar functioning (Raman and Bean, 1999b; Khaliq et al., 2003; Schaller and Caldwell, 2003; Fry, 2006; Levin et al., 2006; Kalume et al., 2007; Liao et al., 2010). Selective genetic deletion of Nav1.6 in Purkinje neurons, for example, attenuates high frequency firing and results in severe motor deficits (Levin et al., 2006).

In addition to rapidly activating and inactivating, transient (I_{NaT}) and non-inactivating, persistent (I_{NaP}), Nav currents, Purkinje neurons, like a number of additional neuronal cell types (Lewis and Raman, 2014), also express a resurgent Nav current (I_{NaR}) component that is revealed on membrane hyperpolarization following depolarizations (Raman and Bean, 1997, 1999b, a, 2001; Khaliq et al., 2003). First identified in Purkinje neurons by Raman and Bean (1997), I_{NaR} was proposed to result from a process that parallels (and competes with) Nav channel inactivation in which Nav channels, opened on depolarization, are blocked by an endogenous particle (Raman and Bean, 2001). Although this ‘open-blocked’ state is, like the inactivated state, non-conducting, it is functionally distinct in that, on membrane repolarization, channels are unblocked, resulting in ‘resurgent’ Na^+ influx and membrane depolarization (Raman and Bean, 2001; Lewis and Raman, 2014).

Although Nav1.6 is the primary determinant of I_{NaR} in Purkinje neurons, expression of Nav1.6 is not sufficient to generate I_{NaR} in other types of neurons (Burgess et al., 1995; Raman et al., 1997; Smith et al., 1998; Khaliq et al., 2003). In addition, even in Purkinje neurons, other Nav α subunits contribute to I_{NaR}, at least in the absence of Nav1.6 (Raman et al., 1997; Grieco and Raman, 2004). The expression of I_{NaR}, however, is disrupted by intracellular application of alkaline phosphatase or proteases, suggesting that the endogenous blocking particle is a protein that is molecularly distinct from the Nav α subunit(s) (Grieco et al., 2002; Grieco and Raman, 2004). Speculating that the endogenous blocker might have both positively charged and hydrophobic features, like exogenous Nav channel blockers, Grieco et al. (2005) examined the effects of peptide sequences in the intracellular C terminus of the Nav channel accessory subunit, Navβ4, with these combined properties. These experiments revealed that application of a synthetic peptide, KKLITFILKKTREK, corresponding to the intracellular domain of mouse Navβ4, to trypsin-treated Nav channels in inside-out membrane patches excised from isolated cerebellar Purkinje neurons restored I_{NaR}. In addition, the effects were reversible (Grieco et al., 2005). Further support for an important role of Navβ4 was provided using siRNA mediated "knockdown" of Navβ4 in cultured cerebellar granule neurons (Bant and Raman, 2010). I_{NaR} was eliminated in ~50% of the siRNA-treated granule cells. It was not possible, however, to determine whether the residual I_{NaR} reflected transfection and/or knockdown inefficiency or, alternatively, the presence of other (non-Navβ4) mechanisms to generate I_{NaR}. Interestingly, expression of Nav α subunits with Navβ4 in heterologous cells does not reveal I_{NaR} (Chen et al., 2008; Aman et al., 2009; Theile et al., 2011).

The experiments here were designed to test directly the hypothesis that Navβ4 is *required* for the generation of I_{NaR} in cerebellar Purkinje neurons and to define the physiological role(s) of Navβ4 and Navβ4-mediated I_{NaR} in the regulation of high frequency repetitive firing in these cells. The results demonstrate a role for Navβ4 in controlling the density, but not the time- or voltage-dependent properties, of I_{NaR} in (mouse) cerebellar Purkinje neurons and, in addition, reveal that Navβ4, through regulation of I_{NaR}, functions to control high frequency repetitive firing rates in Purkinje neurons and to maintain normal balance and motor coordination.

RESULTS

Targeted disruption of Scn4b results in impaired motor performance

To define the physiological role of Navβ4 in the generation of I_{NaR}, we developed a mouse (*Scn4b*$^{-/-}$) model lacking *Scn4b*, as described in Experimental Procedures and illustrated in Figure 1A. The *Scn4b*$^{-/-}$ line was validated by comparing *Scn4b* transcript (Figure 1B) and Navβ4 protein in the cerebella of WT and *Scn4b*$^{-/-}$ animals. As illustrated in Figure 1C, Navβ4 is undetectable in *Scn4b*$^{-/-}$ cerebellum. In addition, the expression levels of the transcripts encoding the other Navβ subunits (*Scn1b, 2b and 3b*) and the Navα subunits (*Scn1a, 2a and 8a*) in *Scn4b*$^{-/-}$ cerebella are similar to WT levels. Adult (5–8 week) *Scn4b*$^{-/-}$ animals (male and female) were indistinguishable from WT mice in terms of overall size, weight, feeding behavior and survival. In addition, no differences in fertility or litter sizes were evident. To determine if the loss of *Scn4b* affects motor coordination and/or

balance, we examined the performance of adult animals in the elevated balance beam task (Carter et al., 2001). A cohort of adult (8–9 week) WT (N = 12) and *Scn4b*$^{-/-}$ (N = 11) animals were tested on an 11 mm flat beam and on a 5 mm cylindrical beam on four consecutive days. The time it took the animal to traverse a narrow elevated beam from a clear platform into an enclosed box (see schematic in Figure 1D) and the number of hindlimb foot slips along the way were quantified. The *Scn4b*$^{-/-}$ animals took significantly longer to cross both the 11 mm ($P < 0.0001$) and the 5 mm ($P < 0.01$) beams (Figures 1E, 1F) and had significantly ($P < 0.01$) more hindlimb foot slips on the 5 mm cylindrical beam (Figure 1H, 2-way ANOVA), compared with WT animals.

High frequency firing is attenuated in adult Scn4b$^{-/-}$ Purkinje neurons

Whole-cell recordings obtained from Purkinje neurons in acute slices prepared from adult (5–8 week old) animals revealed that *Scn4b*$^{-/-}$ Purkinje neurons, like WT Purkinje neurons, fire spontaneously and repetitively (Figure 2A). The mean repetitive firing rate in *Scn4b*$^{-/-}$ Purkinje neurons, however, was significantly ($P < 0.001$, Student's *t*-test) lower than in WT Purkinje neurons (Figure 2B). Firing frequency versus injected current (F-I) curves also demonstrate that WT Purkinje neurons fire at significantly ($P < 0.01$, 2-way ANOVA) higher frequencies than *Scn4b*$^{-/-}$ Purkinje neurons in response to current injections of varying amplitudes (Figure 2C–F). The marked differences in firing rates are evident when depolarizing currents are injected from baseline (Figure 2C–D), as well as following hyperpolarizing current injections (Figure 2E–F), delivered to silence the cells and normalize membrane potentials. Although repetitive firing rates are quite different (Figure 2), the properties of individual action potentials in adult WT and *Scn4b*$^{-/-}$ Purkinje neurons are indistinguishable (Table S1).

Acute in-vivo Navβ4 knockdown in mature Purkinje neurons also disrupts high frequency firing

Additional experiments were conducted to determine the functional effects of reducing Navβ4 expression in adult Purkinje neurons using shRNA-mediated knockdown of *Scn4b*. The *Scn4b*-targeted shRNA- or the non-targeted (control) shRNA-expressing AAV1 was injected into the cerebellar vermis of 3–4 week old WT animals and acute cerebellar slices (Figure 3A) were prepared 2–4 weeks later. In *Scn4b*-targeted shRNA-expressing Purkinje neurons, the rate of spontaneous firing was significantly ($P < .01$; Student's *t*-test) reduced (Figure 3B), compared to WT (Figure 2B) or non-targeted shRNA-expressing (Figure 3B–C) cells. The rate of repetitive firing in response to depolarizing current injections was also significantly ($P < .05$, 2-way ANOVA) lower in *Scn4b*-targeted, than in non-targeted shRNA-expressing (Figure 3D–E) Purkinje neurons. Action potential waveforms in *Scn4b*-targeted and non-targeted shRNA-expressing cells were also similar (Table S1).

To determine if *Scn4b* affects the rate at which Purkinje neurons enter a state of depolarization block during high frequency firing, we also measured the duration of firing in response to depolarizing current injections of varying amplitudes (0.5 – 2.5 nA) in WT and *Scn4b*$^{-/-}$ Purkinje neurons, as well as in adult Purkinje neurons expressing the *Scn4b*-targeted shRNA or the non-targeted shRNA. These experiments revealed that neither the deletion of *Scn4b,* nor the *in vivo* knockdown of *Scn4b,* measurably affected the duration of

repetitive firing during depolarizing current injections (Figure S1). Loss of Navβ4, therefore, does not result in changes in the rate of depolarization block (see Discussion).

Effects of the targeted deletion of Scn4b on Nav currents in adult Purkinje neurons

To explore the ionic basis of the attenuation of spontaneous and evoked repetitive firing rates, we examined Nav currents in adult *Scn4b*$^{-/-}$ and WT Purkinje neurons in acute slices. We used a voltage-clamp protocol, developed by Milescu et al. (2010), that mitigates the difficulties inherent in measuring Nav currents in neurons with intact neurites (Raman and Bean, 1999b; Sacco and Tempia, 2002). Briefly, cells were first depolarized with a 'pre-pulse', to inactivate Nav channels in both the soma and distal neurites, and subsequently hyperpolarized to allow recovery from inactivation of channels in/near the soma, regions likely to be adequately voltage-clamped. A third depolarizing step was then delivered to activate the Nav channels in/near the soma (Figure 4A). Analyses of the Nav currents evoked at various test potentials using this protocol revealed that there was a significant ($P < 0.05$, Student's *t*-test) hyperpolarizing shift in the voltage-dependence of activation (G_{NaT}) of the transient component of the current (I_{NaT}) in *Scn4b*$^{-/-}$ ($V_{1/2} = -39.7 \pm 0.6$ mV; n = 13), compared to WT ($V_{1/2} = -34.1 \pm 0.6$ mV; n = 12), Purkinje neurons. In addition, the slope factor of the Boltzmann fit to the G_{NaT} versus voltage plot reflects the steeper voltage-dependence of activation of the Nav current in *Scn4b*$^{-/-}$ (slope factor = 3.7 ± .6), compared with WT (slope factor = 6.8 ± .6), Purkinje neurons (Figure 4B).

To measure the voltage-dependence of steady-state inactivation of I_{NaT} in WT and *Scn4b*$^{-/-}$ Purkinje neurons, a similar three-step protocol was used. Cells were depolarized to inactivate the Nav channels in the soma and distal neurites and subsequently hyperpolarized to varying levels to allow recovery of the channels in/near the soma (Figure 4C). In contrast with current activation, the loss of *Scn4b* did not measurably affect the voltage-dependence of inactivation of I_{NaT} in mature Purkinje neurons (Figure 4D).

The pre-pulse technique was not sufficient to allow reliable measurement of I_{NaR} in Purkinje neurons in slices because the membrane voltage could not be adequately controlled during the much longer (~80 ms) voltage steps needed to record I_{NaR}. It was shown previously, however, that I_{NaR} could be successfully measured in Purkinje neurons in intact cerebellar slices by superfusion of TTX-containing bath solution and subsequent off-line subtraction of the currents measured before and after exposure to TTX (Afshari et al., 2004). Using this approach, we measured TTX-sensitive currents in *Scn4b*$^{-/-}$ Purkinje neurons with a brief depolarizing voltage step to 30 mV, to activate Nav currents, followed by a hyperpolarizing step to −40 mV, to measure I_{NaR}. In 4/4 adult *Scn4b*$^{-/-}$ Purkinje neurons, subtraction of records before and after TTX revealed transient and 'resurgent' TTX-sensitive currents (Figure 4E2), although this strategy did not allow direct determination of the magnitude or the voltage-dependent properties of I_{NaR}.

Peak transient Nav current density is higher in acutely isolated neonatal Scn4b$^{-/-}$, than in WT, Purkinje neurons

Using the prepulse protocol described above, it was not possible to determine how much of the axial Nav current may be contaminating the Nav currents measured in the soma and, in

addition, whether the contamination was variable among cells. If present, contamination from unclamped axial Nav currents could impact the reliable determination of the slopes of the activation and inactivation curves (Figure 4B, 4D). In the slice preparation, it was also not possible to measure the magnitude or the voltage dependence of I_{NaR} accurately. To enable detailed characterization of I_{NaR} and I_{NaT}, therefore, additional voltage-clamp experiments were performed on Purkinje neurons acutely isolated from neonatal (P11–P18) WT and *Scn4b*$^{-/-}$ animals. During the isolation protocol, many (axonal and dendritic) processes are removed, providing more spherical cells (Figure 5A), thereby allowing more reliable spatial control of the membrane voltage and Nav current measurements.

Representative I_{NaT} recordings are presented in Figure 5B. The current-voltage plot in Figure 5C reveals that I_{NaT} densities are *higher* in neonatal *Scn4b*$^{-/-}$, than in WT, Purkinje neurons. I_{NaT} also appeared to be larger in adult *Scn4b*$^{-/-}$ than in WT Purkinje neurons in acute slices (Figure S2). Interestingly, and in contrast to the findings in adult Purkinje neurons, there were no significant differences in spontaneous (Figure S3A–B) or evoked firing (Figure S3C) rates in neonatal *Scn4b*$^{-/-}$ and WT Purkinje neurons, suggesting that defects in repetitive firing associated with the loss of Navβ4 develop as the animals mature (see Discussion).

Although peak I_{NaT} densities were increased, there were no measurable differences in the rates of I_{NaT} inactivation (Figure 5D) or in the voltage-dependences of steady-state inactivation of I_{NaT} (Figure 5F) in neonatal WT and *Scn4b*$^{-/-}$ Purkinje neurons. Similar to the findings in adult cells (Figure 4B), there was a small hyperpolarizing shift in the $V_{1/2}$ of activation of I_{NaT} in *Scn4b*$^{-/-}$ ($V_{1/2}$ = −49.1 ± 0.5 mV; n = 13), compared with WT ($V_{1/2}$ = −47.6 ± 0.6 mV; n = 10), Purkinje neurons (Figure 5E). The voltage-dependence of activation of the persistent component of the Nav current, I_{NaP} (Figure 5G) and the ratio of I_{NaP} to I_{NaT} (Figure 5H), however, were indistinguishable in neonatal *Scn4b*$^{-/-}$ and WT Purkinje neurons. A −80mV voltage step of varying duration was used to determine that the rates of recovery of I_{NaT} from inactivation (Figure 5I) were similar in WT (τ = 3.8 ± .1 ms; n = 8) and *Scn4b*$^{-/-}$ (τ = 3.9 ± .1 ms; n = 7) Purkinje neurons. Action-potential clamp experiments were also conducted to allow the measurement of Nav currents elicited by high-frequency and successive depolarizations and to determine if the time course and extent of cumulative inactivation of Nav currents were altered in *Scn4b*$^{-/-}$, compared with WT, Purkinje neurons. The voltage command used in these experiments was a train of 15 action potentials recorded from an adult Purkinje neuron firing at 95 Hz. No cumulative inactivation of TTX-sensitive Nav currents in neonatal WT (n = 6) and *Scn4b*$^{-/-}$ (n = 7) Purkinje neurons was observed (Figure 5J).

I_{NaR} is attenuated, but not eliminated, in acutely isolated P11–P18 Scn4b$^{-/-}$ Purkinje neurons

Additional experiments were focused on determining directly the effects of the targeted deletion of *Scn4b* on I_{NaR}. Using a bath solution with reduced Na^+ (Raman and Bean, 1997, 1999b), Nav currents evoked during a voltage-ramp (from 20 mV to −100 mV at 2 mV/ms) before and after application of TTX (Figure 6A) were recorded and normalized to the maximal TTX-sensitive current measured at +20 mV (Figure 6B). This protocol revealed

that the ratio of the TTX-sensitive ramp current to I_{NaT} was significantly ($P < 0.01$, Student's *t*-test) higher (0.15 ± 0.02) in WT, than in *Scn4b*$^{-/-}$, Purkinje neurons (0.06 ± 0.01). Although these results clearly suggest the presence of residual I_{NaR} in *Scn4b*$^{-/-}$ Purkinje neurons, the ramp currents actually reflect both I_{NaP} and I_{NaR}, and it is not possible to subtract the contribution of I_{NaP} to isolate I_{NaR}.

To confirm that I_{NaR} is indeed present in *Scn4b*$^{-/-}$ Purkinje neurons and to measure the kinetic properties of the residual currents, it was necessary to clamp the currents using steady-state voltage steps. With 154 mM Na^+ in the bath, I_{NaR} was recorded in response to hyperpolarizing voltage steps presented following membrane depolarization (Figure 6C) before and after TTX application. Analyses of the TTX-sensitive currents revealed that peak I_{NaR} was significantly ($P < .05$, two-way ANOVA) lower in *Scn4b*$^{-/-}$ (−410 ± 53 pA), than in WT (−715 ± 110 pA), Purkinje neurons (Figure 6D, E). The peak I_{NaR} was measured at −50 mV in WT and at −45 mV in *Scn4b*$^{-/-}$ Purkinje neurons. The time constants (tau) of I_{NaR} decay, measured in WT and *Scn4b*$^{-/-}$ Purkinje neurons (at both −20 and −45 mV), were similar (Figure 6F) indicating that, although reduced in amplitude, the time- and voltage-dependent properties of the residual I_{NaR} in *Scn4b*$^{-/-}$ Purkinje neurons are indistinguishable from I_{NaR} in WT Purkinje neurons (see Discussion).

Dynamic clamp-mediated addition of I_{NaR} rescues high frequency firing in Scn4b$^{-/-}$ Purkinje neurons

To explore directly the role of I_{NaR} in regulating the repetitive firing properties of Purkinje neurons, we simulated I_{NaR} using a previously developed Markov model (Figure 7A) of I_{Na} (Raman and Bean, 2001) and isolated the 'resurgent' portion of the current for application with dynamic clamp using the Real Time Experimental Interface (RTXI) software (Lin et al., 2010). To verify that the simulated current was appropriately linked and applied in RTXI, we measured the response of simulated I_{Na} and I_{NaR} to brief depolarizing current injections in a model cell (Supplemental Experimental Procedures). Depolarizing current injections were presented to the model cell to activate I_{Na} (Figure 7B). The RTXI current generated had a large and fast inactivating portion, corresponding to I_{NaT}, and a slowly activating and inactivating portion, corresponding to I_{NaR} (Figure 7B RTXI current). We then applied the condition, illustrated in Figure 7C (*left*), to limit the model to only I_{NaR} and applied identical depolarizing current injections. This resulted in an RTXI current that consisted of only the slowly activating and inactivating portion of I_{Na}, i.e., I_{NaR} (Figure 7C, *right*). We also measured I_{Na} in isolated Purkinje neurons under control conditions and with the modeled I_{Na} added. As illustrated in Figure S4, the model performed appropriately, adding inward currents with transient and resurgent Nav current components.

With the model validated, we used RTXI to add I_{NaR} during whole-cell current-clamp recordings from adult *Scn4b*$^{-/-}$ Purkinje neurons in acute slices. To determine the effects of I_{NaR} on repetitive firing, we added a nominal I_{NaR} that peaked at 150 pA during the action potential and administered a current-clamp protocol that applied various depolarizing current injections. In each Purkinje neuron tested, I_{NaR} was applied at 1x, 2x, 4x and 8x the nominal (150 pA) value and identical current-clamp protocols were administered. These experiments revealed that the addition of I_{NaR} increased the spontaneous firing rates of *Scn4b*$^{-/-}$ Purkinje

neurons and, in addition, that the firing frequency was positively correlated with the magnitude of I_{NaR} added (Figure 7D). We also explored the activation properties of I_{NaR} during the action potential and its relation to the firing rate. We found that I_{NaR} is activated during the repolarizing phase of the action potential, reflecting activation at hyperpolarized membrane potentials (Raman and Bean, 1997, 1999b). In addition, I_{NaR} is active during the interspike interval (Figure 7E, *upper traces*, *red arrow*) (Khaliq et al., 2003) and, when cells are firing at high rates (>100 Hz), I_{NaR} also contributes to the upswing (depolarizing phase) of the subsequent action potential (Figure 7E *lower traces*, *blue arrow*). In light of these observations, we thought it was also important to verify that the RTXI current applied during the upswing of the action potential was indeed I_{NaR}.

In the model (Figure 7A), I_{NaR} is the simulated current resulting from channels moving from the 'open-blocked' (OB) state into the 'open' (O) state. To determine if only I_{NaR} is being applied, we first analyzed the proportion of channels in each kinetic state, in real-time, with Purkinje neuron action potentials and RTXI current injections. This analysis revealed that, during the upswing of an action potential, the proportion of channels in the 'OB' state was decreasing, while the proportions of channels in the 'O' and 'C5' states were increasing, indicating that during the upswing of the action potential, the RTXI current, at least partially, reflects I_{NaR} (Figure 7F). If the current injected during the upswing of the action potential is indeed I_{NaR}, then hyperpolarizing the membrane should reduce, and eventually eliminate, the current because at more hyperpolarized potentials, the rate constant for transitioning from the 'OB' state to the 'O' state increases (Raman and Bean, 2001). At more hyperpolarized potentials, therefore, I_{NaR} decays more quickly and is more likely to be eliminated before the onset of the subsequent action potential. To test this hypothesis, we applied the I_{NaR} model during recordings of action potentials from a Purkinje neuron offline using Matlab (Mathworks). Specifically, we hyperpolarized the recorded action potentials by fixed voltages and analyzed the magnitudes of I_{NaR} activated (Figure 7G). These simulations revealed that, successive hyperpolarizations of the membrane voltage reduced, and eventually eliminated, I_{NaR} during the action potential upstroke, consistent with the suggestion that the current reflects channels moving from the 'OB' state to the 'O' state and also with the hypothesis that the current injected during the upstroke is indeed I_{NaR}. It should be noted that, although these experiments clearly suggest that I_{NaT} was not contaminating the dynamic clamp mediated I_{NaR}, I_{NaP} was not subtracted from the inserted currents and may have had depolarizing effects early during the inter-spike interval. In addition, because activation of the transient and resurgent Nav currents can occur simultaneously, the modeled I_{NaR} added via the dynamic clamp might be an underestimate of the magnitude of I_{NaR} present during the upswing and initial downswing of the action potentials.

DISCUSSION

Navβ4 and I_{NaR} in the regulation of high frequency firing in Purkinje neurons

It has been reported that the rate of recovery from inactivation of the transient Nav current is faster in cells, such as Purkinje neurons, with I_{NaR} than in cells, such as CA1 hippocampal pyramidal neurons, that do not express I_{NaR} (Raman and Bean, 1997). These observations

have been interpreted as suggesting that the open blocked state, by competing with conventional Nav channel inactivation, supports rapid recovery from inactivation and thus facilitates high-frequency action-potential generation indirectly (Raman and Bean, 2001). Here, we show that loss of Navβ4 attenuates repetitive firing rates in adult Purkinje neurons, a decrease that could be due to reduced I_{NaR}, more Nav channels entering the inactivated state, or both. To distinguish among these, we analyzed the rate at which cells enter a state of depolarization-block in response to current injections of varying amplitudes. These experiments revealed that the amount of time it took for cells to stop firing was similar in adult *Scn4b*$^{-/-}$, *Scn4b*-shRNA-expressing and WT Purkinje neurons (Figure S1). In voltage-clamp experiments on neonatal *Scn4b*$^{-/-}$ and WT Purkinje neurons, we also found that loss of Navβ4 did not affect the rate of recovery from inactivation or the cumulative inactivation of Nav currents during high frequency depolarizations. These observations suggest that the repetitive firing rates of Purkinje neurons lacking Navβ4 are attenuated because of the loss of I_{NaR} and not because of additional Nav channels being absorbed into inactivated states.

The hypothesis that reduced I_{NaR} underlies the attenuation in spontaneous and evoked repetitive firing rates in adult *Scn4b*$^{-/-}$ Purkinje neurons is further supported by the dynamic clamp experiments, showing that addition of I_{NaR} increased spontaneous and evoked firing rates. Importantly, firing rates “scaled” to the amplitude/density of the dynamic clamp-mediated addition of I_{NaR} and repetitive firing was partially “rescued” to WT Purkinje neuron levels. These dynamic clamp experiments also revealed that, when mature Purkinje neurons fire at high frequencies, I_{NaR} provides depolarizing drive not only during the repolarization phase of the action-potential, but also during the inter-spike interval and the upstroke of the subsequent action-potential.

Motor defects which may be attributed to reduced repetitive firing rates in Purkinje neurons, were observed in adult *Scn4b*$^{-/-}$ animals. Global deletion of Navβ4, however, may affect motor performance through other pathways. It has been reported, for example (Miyazaki et al., 2014), that loss of Navβ4 disrupts firing in medium spiny neurons of the striatum, which is also involved in action selection and motor control.

Acute *in vivo* knockdown of Navβ4 in mature Purkinje neurons

Spontaneous high frequency firing was also observed in adult *Scn4b*-targeted shRNA-expressing Purkinje neurons and repetitive firing rates were further increased by depolarizing current injections. In addition, both spontaneous and evoked repetitive firing rates were significantly lower in *Scn4b*-targeted shRNA-, compared with non-targeted *shRNA-,* expressing adult cerebellar Purkinje neurons. The repetitive firing properties of adult *Scn4b*-shRNA-expressing and *Scn4b*$^{-/-}$ Purkinje neurons, however, were indistinguishable. These observations demonstrate a physiological role for Navβ4 in regulating the repetitive firing properties of mature Purkinje neurons that is independent of any developmental function(s) of Navβ4. In addition, these results, together with the dynamic-clamp results, lead us to conclude that the lack of Navβ4 throughout development does not result in any secondary changes in membrane properties that impact the repetitive firing properties of cerebellar Purkinje neurons.

There were, however, clear differences in the impact of the loss of Navβ4 on the firing properties of neonatal, compared with adult, *Scn4b*$^{-/-}$ Purkinje neurons. In contrast with the findings in adult animals, the spontaneous and evoked repetitive firing rates of neonatal *Scn4b*$^{-/-}$ and WT Purkinje neurons were indistinguishable. These differences may reflect development change(s) in the pore forming or accessory subunits contributing to functional Purkinje neuron Nav channels. Developmental changes in the expression (densities) and/or the properties of the other channels contributing to action potential generation and controlling repetitive firing rates could also play a role.

Loss of Navβ4 reduces, but does not eliminate, I_{NaR} in cerebellar Purkinje neurons

The voltage-clamp experiments here revealed that I_{NaR} amplitudes were attenuated in neonatal *Scn4b*$^{-/-}$ Purkinje neurons, although I_{NaR} was not eliminated. Indeed, I_{NaR} amplitudes in *Scn4b*$^{-/-}$ Purkinje neurons were ~ 50% of WT I_{NaR} amplitudes. In Bant and Raman (2010), siRNA-mediated knockdown of Navβ4 in cultured granule neurons resulted in a 59% reduction in the mean I_{NaR}, similar to what is reported here. In Bant and Raman (2010), however, I_{NaR} was eliminated in 9 of the 18 granule cells expressing siRNAs targeting *Scn4b*, whereas we found no *Scn4b*$^{-/-}$ Purkinje neurons lacking I_{NaR}. In addition, the acute *in vitro* knockdown of *Scn4b* in granule cells also reduced I_{NaP} and shifted (in the hyperpolarizing direction) the voltage-dependence of inactivation of I_{NaT}. Neither of these effects were observed with loss of *Scn4b* in Purkinje neurons. Acute, *in vitro* knockdown of Navβ4 in dorsal root ganglion neurons also markedly reduced (from ~80% to ~35%) the percentage of cells with detectable I_{NaR}, i.e., expression of the Navβ4-targeted siRNA eliminated I_{NaR} in ~40% of the cells (Barbosa et al., 2015). Taken together, these results suggest that there are cell-type specific differences in the mechanisms that generate I_{NaR} and, in addition, that there may be heterogeneity in a given cell type.

The finding of robust expression of I_{NaR} in *Scn4b*$^{-/-}$ Purkinje neurons clearly indicates that there are additional intrinsic mechanism(s) in these cells that contribute to the generation of I_{NaR} or, alternatively, are capable of generating I_{NaR} in the absence of Navβ4. Previous studies have suggested that the kinetic properties of I_{NaR} are dependent on the Nav α subunit(s) encoding the currents (Do and Bean, 2004; Aman and Raman, 2007; Kalume et al., 2007; Lewis and Raman, 2011). Here, however, the time- and voltage-dependent properties of I_{NaR}, measured in *Scn4b*$^{-/-}$ and WT Purkinje neurons were not significantly different, suggesting that the same Nav α subunit or subunits generate I_{NaR} in the absence and in the presence of Navβ4.

Clearly, the question then is: what underlies the generation of the resurgent Nav current evident in *Scn4b*$^{-/-}$ Purkinje neurons? The simplest hypothesis would be that there are additional protein(s) that function, perhaps only in the absence of Navβ4, to block open Nav channels at depolarized potentials. One candidate protein is Navβ2, which shares 35% sequence identity with Navβ4 (Yu et al., 2003), and a similar, conserved C-terminal tail (Lewis and Raman, 2014). When co-expressed with Nav1.1 in HEK-293 cells, Navβ2 produces effects on Nav currents similar to those seen with Navβ4 (Aman et al., 2009) and, like Navβ4, Navβ2 forms disulfide bonds with Nav α subunits *in situ* (Chen et al., 2012). In addition, the C-terminal tail of Navβ2 contains several positively charged residues, which

are necessary for open-channel block (Lewis and Raman, 2011). A phenylalanine residue that is conserved in the C-terminal tails of Navβ4 in multiple species and that is thought to stabilize open-channel block, however, is absent in Navβ2. In addition, unlike Navβ4, overexpression of Navβ2 in dorsal root ganglion neurons had no effect on the magnitude or properties of I_{NaR} (Barbosa et al., 2015).

An alternative hypothesis is that there are other mechanisms, distinct from open-channel block, that contribute to the generation of I_{NaR} in Purkinje neurons under basal conditions or, alternatively, only in the absence of Navβ4. There could, for example, be an intrinsic mechanism, perhaps another channel regulatory protein that interacts with the voltage-sensor domains of Nav α subunits and modifies (slows) channel deactivation, as has been shown to occur with β-toxins from *Centruroides* scorpions (Cahalan, 1975). The β-scorpion toxin, Cn2, from *Centruroides noxius*, for example, "traps" the S4 voltage sensor segment in domain II of Nav α subunits, and produces resurgent Nav currents in HEK-293 cells stably expressing human Nav1.6 (Schiavon et al., 2006). In addition, Cn2 produces resurgent Nav currents in (rat) cerebellar Purkinje neurons although, interestingly, the voltage-dependent properties of the toxin-generated resurgent current are distinct from native I_{NaR} (Schiavon et al., 2006). Another, related β-toxin was subsequently shown to produce resurgent Nav currents in HEK-293 cells stably expressing other (i.e., in addition to Nav1.6) Nav α subunits (Schiavon et al., 2012). Although no intrinsic modulators of Nav channels with properties similar to the scorpion β-toxins have been identified to date, it is interesting to note that a missense mutation in *SCN11A* (Nav1.9) in a patient with painful small fiber neuropathy was identified (G699R) that results in substitution of glycine 699 by arginine (Han et al., 2015). In addition to affecting the voltage-dependences of channel activation and inactivation, the G699R mutation slows the rate of Nav1.9 channel deactivation and renders dorsal root ganglion neurons hyperexcitable (Han et al., 2015). These combined observations clearly suggest that additional intrinsic mechanisms can modify Nav channel gating and contribute to the generation resurgent Nav currents.

EXPERIMENTAL PROCEDURES

All reagents were obtained from Sigma Aldrich unless otherwise noted.

Animals

All experiments involving animals were performed in accordance with the guidelines published in the National Institutes of Health's *Guide for the Care and Use of Laboratory Animals* and all protocols were approved by the Washington University Animal Studies Committee. Wild type (WT) C57Bl/6J mice were obtained from Jackson Laboratories. The *Scn4b*$^{-/-}$ mouse line was generated in the Department of Pathology and Immunology Transgenic Knockout and Microinjection Core. The *Scn4b* locus on mouse chromosome 9 contains 5 exons that encode the 228 amino acid Navβ4 protein. Zinc finger nucleases (ZFN) targeting exon 3 of *Scn4b* were designed and validated by Sigma-Aldrich. Pronuclei of C57Bl/6J fertilized eggs were injected with RNA encoding the ZFN and 12 of the 23 pups born contained a mutation in *Scn4b* as detected by a CelI mismatch assay (Oleykowski et al., 1998). A mutated allele that contained a 10 base pair deletion, resulting in a frameshift and a

stop codon at residue 137 (Figure 1A) was identified. *Scn4b*$^{+/-}$ mice were backcrossed into C57Bl/6J and then crossed to generate the *Scn4b*$^{-/-}$ line. All experiments were performed on both male and female animals.

Acute *in vivo* knockdown of *Scn4b*

Four *Scn4b* shRNAs were screened in TSA-201 cells co-expressing Navβ4-YFP (see Supplemental Experimental Procedures). Western blot analysis of lysates from these cells revealed that one of these shRNAs (5′-CCAGCTGTTATGGCTTTGAGA-3′) reduced Navβ4 expression by >50%. This shRNA and a non-targeted control shRNA sequence were then cloned (individually) in an miR-30 context into the 3′-UTR of tdTomato (Norris et al., 2010), inserted into an adenoviral shuttle vector containing the CAG promoter and adeno-associated viruses serotype 1 (AAV1), previously shown to provide selective expression in cerebellar Purkinje neurons *in situ* (Bosch et al., 2015), were generated. shRNA- and non-targeting control expressing AAV1 viruses were injected into the cerebellar vermis of WT animals as described in Bosch et al. (2015) and in the Supplemental Experimental Procedures.

Balance beam

Motor coordination was evaluated blind to genotype by assessing the ability of 8–9 week old (WT and *Scn4b*$^{-/-}$) mice to traverse an 80 cm texturized (5 mm) cylindrical metal beam or an 80 cm texturized (11 mm) flat metal beam to reach an enclosed black plexiglass (20 cm × 20 cm × 20 cm) escape box (Carter et al., 2001), as described in Bosch et al. (2015) and in the Supplemental Experimental Procedures.

Preparation of acute cerebellar slices

Acute cerebellar slices were prepared from (2–8 week old) WT and *Scn4b*$^{-/-}$ animals as previously described (Bosch et al., 2015). Briefly, animals were anesthetized with 1.25% Avertin and perfused transcardially with ice-cold cutting solution containing (in mM): 240 sucrose, 2.5 KCl, 1.25 NaH_2PO_4, 25 $NaHCO_3$, 0.5 $CaCl_2$, and 7 $MgCl_2$, saturated with 95% O_2/5% CO_2. Brains were rapidly removed and parasagittal sections (350μm) were cut on a VT1000 S vibratome (Leica Microsystems) and incubated in oxygenated artificial cerebral spinal fluid (ACSF) containing (in mM): 125 NaCl, 2.5 KCl, 1.25 NaH_2PO_4, 25 $NaHCO_3$, 2 $CaCl_2$, 1 $MgCl_2$, and 25 dextrose (~310 mosmol l^{-1}) for 25 minutes at 33°C and then at 22–23°C for at least 35 min before transfer to the recording chamber.

Isolation of neonatal cerebellar Purkinje neurons

WT and *Scn4b*$^{-/-}$ Purkinje neurons were isolated from P11–P18 animals using described methods (Raman and Bean, 1997) and described in the Supplemental Experimental Procedures.

Electrophysiological recordings

Whole-cell current- and voltage-clamp recordings were obtained from cerebellar Purkinje neurons acutely isolated or in acute slices prepared from young (P14–P15) and adult (5–8 week) WT and *Scn4b*$^{-/-}$ animals using a Multiclamp 700B patch-clamp amplifier interfaced

with a Digidata 1322A acquisition system and pClamp10 software (Molecular Devices) to a Windows 7 PC. Signals were acquired at 50 or 100 kHz and filtered at 10 kHz before storage. Cerebellar slices were continually perfused with oxygenated ACSF at 33 ± 1°C. Input resistances were calculated from a two-sweep voltage clamp protocol in which cells were stepped from a holding potential of −70mV to −80mV and to −60mV. Current- and voltage-clamp protocols and techniques are described in the Supplemental Experimental Procedures.

Dynamic clamp

The recording conditions used in current-clamp experiments were also used in dynamic clamp experiments. In addition to being digitized by the Digidata 1322 A, the voltage signal was digitized with a NI PCI-6010 DAQ card (National Instruments) and stored on another PC running the 64-bit real-time Linux kernel (RTAI). Simulated I_{NaR} was calculated using the RTXI software and converted to an analog signal using the PCI-6010 DAQ card. The output signals of Clampex 10 software (used to run current-clamp protocols) and RTXI software (used to add simulated I_{NaR}) were combined using a voltage summing junction box built by Washington University Electronics Shop. Liquid junctional potentials were corrected (RTXI software) prior to calculations of simulated I_{NaR}.

Simulated I_{NaR}

A thirteen state Markov model of Nav channel gating in Purkinje neurons, based on the model in Raman and Bean (2001) was implemented. This model consists of five closed states (C1–C5), six inactivated states (I1–I6), a single open conductive state (O), and one open-blocked state (OB); a schematic of the model is shown in Figure 7A. The approaches used with this model to determine and apply I_{NaR} in dynamic clamp experiments are described in the Supplemental Experimental Procedures.

Statistical analysis

Results are presented as means ± SEM. In the Figure legends, the numbers of animals (N) and the numbers of cells (n) used in each experiment are provided. Statistical tests performed included the Student's *t* test (unpaired), two-way ANOVA or repeated measures two-way ANOVA, as noted in the text. The D'Agostino-Pearson omnibus test for normality was used to determine that basal firing rate variability was normally distributed in each experimental group.

Supplementary Material

Refer to Web version on PubMed Central for supplementary material.

Acknowledgments

The authors thank Drs. I. Raman, T. Hermanstyne and S. Springer for helpful discussions. Dr. A. Burkhalter for assistance with stereotaxic surgery. We also thank R. Wilson, R.L. Mellor, D. Kreamalmeyer, and S. Horvath for expert technical assistance. Financial support provided by the NIH (R01NS065761 to JMN, F32NS090765 to JLR, and R01AI024157 to PMA) is also gratefully acknowledged. Interfering RNAs (RNAi) were obtained from the RNAi Core, supported by the Genome Institute and the Children's Discovery Institute (CDI-LI-2010-94) at

Washington University, and all viruses were generated in the Hope Center Viral Vectors Core, supported by a Neuroscience Blueprint Core grant (P30 NS057105).

References

Afshari FS, Ptak K, Khaliq ZM, Grieco TM, Slater NT, McCrimmon DR, Raman IM. Resurgent Na currents in four classes of neurons of the cerebellum. J Neurophysiol. 2004; 92:2831–2843. [PubMed: 15212420]

Aman TK, Grieco-Calub TM, Chen C, Rusconi R, Slat EA, Isom LL, Raman IM. Regulation of persistent Na current by interactions between beta subunits of voltage-gated Na channels. J Neurosci. 2009; 29:2027–2042. [PubMed: 19228957]

Aman TK, Raman IM. Subunit dependence of Na channel slow inactivation and open channel block in cerebellar neurons. Biophys J. 2007; 92:1938–1951. [PubMed: 17189307]

Bant JS, Raman IM. Control of transient, resurgent, and persistent current by open-channel block by Na channel beta4 in cultured cerebellar granule neurons. Proc Natl Acad Sci U S A. 2010; 107:12357–12362. [PubMed: 20566860]

Barbosa C, Tan ZY, Wang R, Xie W, Strong JA, Patel RR, Vasko MR, Zhang JM, Cummins TR. Navbeta4 regulates fast resurgent sodium currents and excitability in sensory neurons. Mol Pain. 2015; 11:60. [PubMed: 26408173]

Billard JM, Vigot R, Batini C. GABA, THIP and baclofen inhibition of Purkinje cells and cerebellar nuclei neurons. Neurosci Res. 1993; 16:65–69. [PubMed: 8387166]

Bosch MK, Carrasquillo Y, Ransdell JL, Kanakamedala A, Ornitz DM, Nerbonne JM. Intracellular FGF14 (iFGF14) Is Required for Spontaneous and Evoked Firing in Cerebellar Purkinje Neurons and for Motor Coordination and Balance. J Neurosci. 2015; 35:6752–6769. [PubMed: 25926453]

Burgess DL, Kohrman DC, Galt J, Plummer NW, Jones JM, Spear B, Meisler MH. Mutation of a new sodium channel gene, Scn8a, in the mouse mutant 'motor endplate disease'. Nat Genet. 1995; 10:461–465. [PubMed: 7670495]

Cahalan MD. Modification of sodium channel gating in frog myelinated nerve fibres by Centruroides sculpturatus scorpion venom. J Physiol. 1975; 244:511–534. [PubMed: 1079869]

Carter RJ, Morton J, Dunnett SB. Motor coordination and balance in rodents. Curr Protoc Neurosci. 2001; Chapter 8(Unit 8):12.

Chen C, Calhoun JD, Zhang Y, Lopez-Santiago L, Zhou N, Davis TH, Salzer JL, Isom LL. Identification of the cysteine residue responsible for disulfide linkage of Na+ channel alpha and beta2 subunits. J Biol Chem. 2012; 287:39061–39069. [PubMed: 22992729]

Chen Y, Yu FH, Sharp EM, Beacham D, Scheuer T, Catterall WA. Functional properties and differential neuromodulation of Na(v)1.6 channels. Mol Cell Neurosci. 2008; 38:607–615. [PubMed: 18599309]

Do MT, Bean BP. Sodium currents in subthalamic nucleus neurons from Nav1.6-null mice. J Neurophysiol. 2004; 92:726–733. [PubMed: 15056687]

Fry M. Developmental expression of Na+ currents in mouse Purkinje neurons. Eur J Neurosci. 2006; 24:2557–2566. [PubMed: 17100843]

Gauck V, Jaeger D. The control of rate and timing of spikes in the deep cerebellar nuclei by inhibition. J Neurosci. 2000; 20:3006–3016. [PubMed: 10751453]

Grieco TM, Afshari FS, Raman IM. A role for phosphorylation in the maintenance of resurgent sodium current in cerebellar purkinje neurons. J Neurosci. 2002; 22:3100–3107. [PubMed: 11943813]

Grieco TM, Malhotra JD, Chen C, Isom LL, Raman IM. Open-channel block by the cytoplasmic tail of sodium channel beta4 as a mechanism for resurgent sodium current. Neuron. 2005; 45:233–244. [PubMed: 15664175]

Grieco TM, Raman IM. Production of resurgent current in NaV1.6-null Purkinje neurons by slowing sodium channel inactivation with beta-pompilidotoxin. J Neurosci. 2004; 24:35–42. [PubMed: 14715935]

Han C, Yang Y, de Greef BT, Hoeijmakers JG, Gerrits MM, Verhamme C, Qu J, Lauria G, Merkies IS, Faber CG, Dib-Hajj SD, Waxman SG. The Domain II S4–S5 Linker in Nav1.9: A Missense

Mutation Enhances Activation, Impairs Fast Inactivation, and Produces Human Painful Neuropathy. Neuromolecular Med. 2015; 17:158–169. [PubMed: 25791876]

Kalume F, Yu FH, Westenbroek RE, Scheuer T, Catterall WA. Reduced sodium current in Purkinje neurons from Nav1.1 mutant mice: implications for ataxia in severe myoclonic epilepsy in infancy. J Neurosci. 2007; 27:11065–11074. [PubMed: 17928448]

Khaliq ZM, Gouwens NW, Raman IM. The contribution of resurgent sodium current to high-frequency firing in Purkinje neurons: an experimental and modeling study. J Neurosci. 2003; 23:4899–4912. [PubMed: 12832512]

Levin SI, Khaliq ZM, Aman TK, Grieco TM, Kearney JA, Raman IM, Meisler MH. Impaired motor function in mice with cell-specific knockout of sodium channel Scn8a (NaV1.6) in cerebellar purkinje neurons and granule cells. J Neurophysiol. 2006; 96:785–793. [PubMed: 16687615]

Lewis AH, Raman IM. Cross-species conservation of open-channel block by Na channel beta4 peptides reveals structural features required for resurgent Na current. J Neurosci. 2011; 31:11527–11536. [PubMed: 21832183]

Lewis AH, Raman IM. Resurgent current of voltage-gated Na(+) channels. J Physiol. 2014; 592:4825–4838. [PubMed: 25172941]

Liao Y, Anttonen AK, Liukkonen E, Gaily E, Maljevic S, Schubert S, Bellan-Koch A, Petrou S, Ahonen VE, Lerche H, Lehesjoki AE. SCN2A mutation associated with neonatal epilepsy, late-onset episodic ataxia, myoclonus, and pain. Neurology. 2010; 75:1454–1458. [PubMed: 20956790]

Lin RJ, Bettencourt J, Wha Ite J, Christini DJ, Butera RJ. Real-time experiment interface for biological control applications. Conf Proc IEEE Eng Med Biol Soc. 2010; 2010:4160–4163. [PubMed: 21096883]

Milescu LS, Bean BP, Smith JC. Isolation of somatic Na+ currents by selective inactivation of axonal channels with a voltage prepulse. J Neurosci. 2010; 30:7740–7748. [PubMed: 20519549]

Miyazaki H, Oyama F, Inoue R, Aosaki T, Abe T, Kiyonari H, Kino Y, Kurosawa M, Shimizu J, Ogiwara I, Yamakawa K, Koshimizu Y, Fujiyama F, Kaneko T, Shimizu H, Nagatomo K, Yamada K, Shimogori T, Hattori N, Miura M, Nukina N. Singular localization of sodium channel beta4 subunit in unmyelinated fibres and its role in the striatum. Nat Commun. 2014; 5:5525. [PubMed: 25413837]

Norris AJ, Foeger NC, Nerbonne JM. Interdependent roles for accessory KChIP2, KChIP3, and KChIP4 subunits in the generation of Kv4-encoded IA channels in cortical pyramidal neurons. J Neurosci. 2010; 30:13644–13655. [PubMed: 20943905]

Oleykowski CA, Bronson Mullins CR, Godwin AK, Yeung AT. Mutation detection using a novel plant endonuclease. Nucleic Acids Res. 1998; 26:4597–4602. [PubMed: 9753726]

Raman IM, Bean BP. Resurgent sodium current and action potential formation in dissociated cerebellar Purkinje neurons. J Neurosci. 1997; 17:4517–4526. [PubMed: 9169512]

Raman IM, Bean BP. Ionic currents underlying spontaneous action potentials in isolated cerebellar Purkinje neurons. J Neurosci. 1999a; 19:1663–1674. [PubMed: 10024353]

Raman IM, Bean BP. Properties of sodium currents and action potential firing in isolated cerebellar Purkinje neurons. Ann N Y Acad Sci. 1999b; 868:93–96. [PubMed: 10414287]

Raman IM, Bean BP. Inactivation and recovery of sodium currents in cerebellar Purkinje neurons: evidence for two mechanisms. Biophys J. 2001; 80:729–737. [PubMed: 11159440]

Raman IM, Sprunger LK, Meisler MH, Bean BP. Altered subthreshold sodium currents and disrupted firing patterns in Purkinje neurons of Scn8a mutant mice. Neuron. 1997; 19:881–891. [PubMed: 9354334]

Sacco T, Tempia F. A-type potassium currents active at subthreshold potentials in mouse cerebellar Purkinje cells. J Physiol. 2002; 543:505–520. [PubMed: 12205185]

Schaller KL, Caldwell JH. Expression and distribution of voltage-gated sodium channels in the cerebellum. Cerebellum. 2003; 2:2–9. [PubMed: 12882229]

Schiavon E, Pedraza-Escalona M, Gurrola GB, Olamendi-Portugal T, Corzo G, Wanke E, Possani LD. Negative-shift activation, current reduction and resurgent currents induced by beta-toxins from Centruroides scorpions in sodium channels. Toxicon. 2012; 59:283–293. [PubMed: 22200496]

Schiavon E, Sacco T, Cassulini RR, Gurrola G, Tempia F, Possani LD, Wanke E. Resurgent current and voltage sensor trapping enhanced activation by a beta-scorpion toxin solely in Nav1.6 channel. Significance in mice Purkinje neurons. J Biol Chem. 2006; 281:20326–20337. [PubMed: 16702217]

Smith MR, Smith RD, Plummer NW, Meisler MH, Goldin AL. Functional analysis of the mouse Scn8a sodium channel. J Neurosci. 1998; 18:6093–6102. [PubMed: 9698304]

Theile JW, Jarecki BW, Piekarz AD, Cummins TR. Nav1.7 mutations associated with paroxysmal extreme pain disorder, but not erythromelalgia, enhance Navbeta4 peptide-mediated resurgent sodium currents. J Physiol. 2011; 589:597–608. [PubMed: 21115638]

Yu FH, Westenbroek RE, Silos-Santiago I, McCormick KA, Lawson D, Ge P, Ferriera H, Lilly J, DiStefano PS, Catterall WA, Scheuer T, Curtis R. Sodium channel beta4, a new disulfide-linked auxiliary subunit with similarity to beta2. J Neurosci. 2003; 23:7577–7585. [PubMed: 12930796]

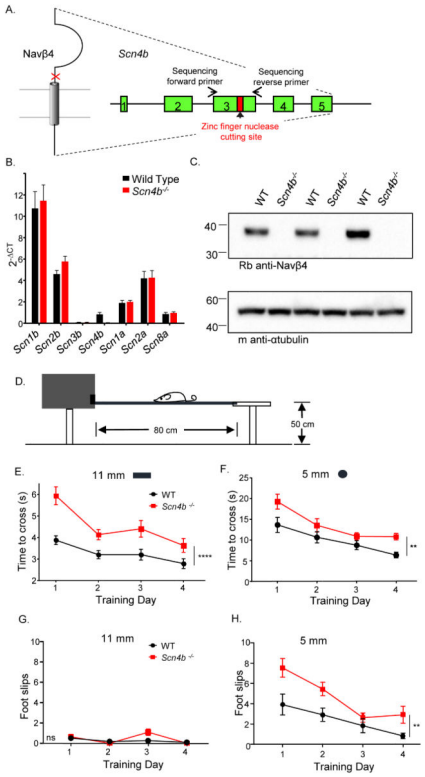

Figure 1. Targeted disruption of *Scn4b* results in impaired motor performance

A, Schematic of the approach used to disrupt the *Scn4b* locus *B,* Nav channel α and β subunit transcript expression levels in cerebellar lysates from *Scn4b*$^{-/-}$ and WT animals. *C,* Western blots of lysates prepared from the cerebella of WT and *Scn4b*$^{-/-}$ animals probed with a polyclonal anti-Navβ4 (AbCam) antibody. *D,* Balance and motor coordination were evaluated by quantifying performance on the elevated balance beam (see Experimental Procedures). *E–F,* The mean ± SEM times to cross the 11 mm (*E*) and the 5 mm (*F*) beams, however, were significantly (***** P < .0001*; ** *P* < .01; two-way ANOVA) longer for the *Scn4b*$^{-/-}$ (N = 11), than the WT (N = 12), animals. *G–H,* Analysis of the numbers of hindlimb footslips revealed very few placement errors for both *Scn4b*$^{-/-}$ and WT animals on the 11 mm beam, whereas the *Scn4b*$^{-/-}$ animals had significantly (*P* < .01; two-way ANOVA) more footslips than WT animals on the 5 mm beam.

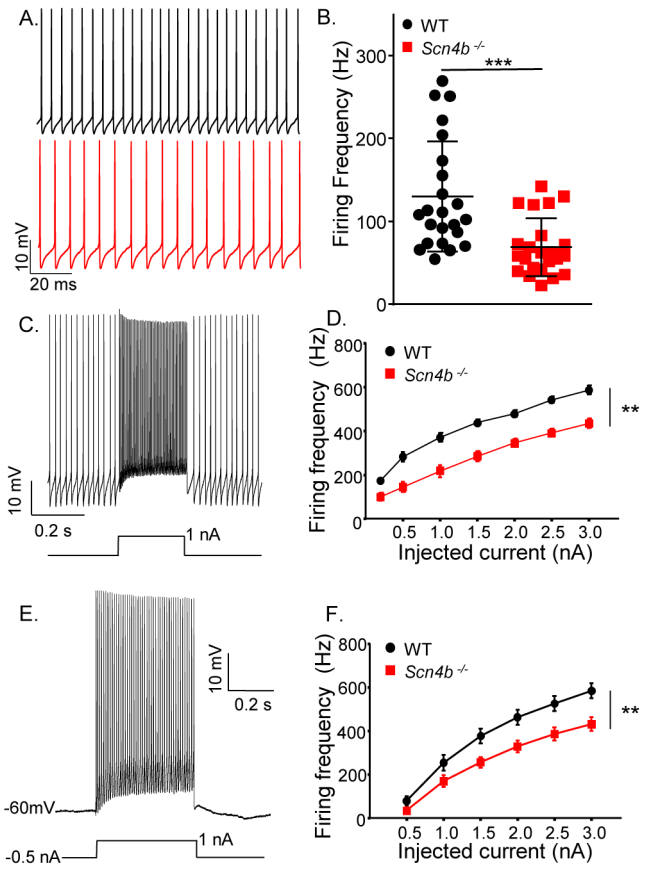

Figure 2. High frequency firing is attenuated in adult *Scn4b*$^{-/-}$ Purkinje neurons

A, Representative whole-cell recordings obtained from adult WT (*upper, black*) and *Scn4b*$^{-/-}$ (*lower, red*) Purkinje neurons in acute cerebellar slices. *B*. The mean ± SEM spontaneous firing frequency measured in adult *Scn4b*$^{-/-}$ (*red*; N = 5, n = 23) Purkinje neurons was significantly (*** $P < .001$; Student's *t*-test) lower than in WT (*black*; N = 5, n = 23) cells. *C–F,* Repetitive firing rates in response to depolarizing current injections from the baseline (*C, D*) and following a (−0.5 nA) hyperpolarizing current injection (*E,* F) were also measured. Representative recordings from WT Purkinje neurons are shown in *C* and *E*; the protocols are displayed below the records. Mean ± SEM evoked firing rates were significantly (** $P < .01$; two-way ANOVA) lower in *Scn4b*$^{-/-}$ (N = 4, n = 10–14), than in WT (N = 3, n = 12–16), Purkinje neurons both at baseline (*D*) and following the −0.5 nA prepulse (*F*). See also Figure S3.

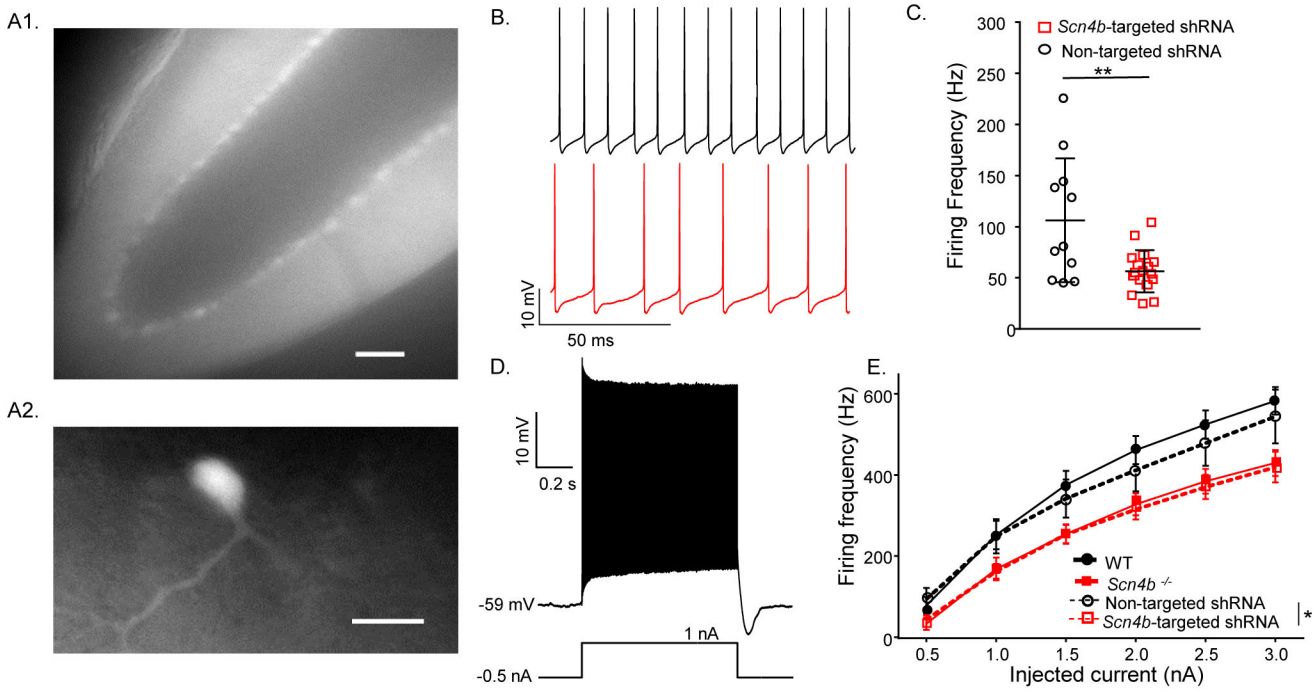

Figure 3. Acute in-vivo Navβ4 knockdown in mature Purkinje neurons also disrupts high frequency firing

A, Representative fluorescence images of an acute cerebellar slice prepared from a WT adult mouse 3 weeks following injection of *Scn4b*-targeted shRNA-expressing AAV1. The low magnification image (*A1*) shows widespread tdTomato expression throughout an entire lobule of the cerebellum (*scale bar = 100 μm*) and the higher magnification image (*A2*) shows a single AAV1-transduced Purkinje neuron (*scale bar = 50 μm*). *B,* Representative current-clamp recordings from td-Tomato-expressing Purkinje neurons in slices prepared two weeks following injections of the non-targeted shRNA- (*upper; black*) or the *Scn4b*-targeted shRNA- (*lower; red*) expressing AAV1. *C,* Purkinje neurons expressing the *Scn4b*-targeted shRNA (*red;* N = 2; n = 17) fired at significantly (** $P < .01$; Student's *t*-test) lower rates than cells expressing the non-targeted shRNA (*black;* N = 2; n = 11). *D,* Repetitive firing rates in response to varying amplitude depolarizing current injections following −0.5 nA prepulses were measured in experiments similar to those in Figure 2F. *E,* Mean ± SEM evoked firing rates are significantly (* $P < .05$, *two-way ANOVA*) lower in Purkinje neurons expressing the *Scn4b*-targeted shRNA (N = 2; n = 13, *red dashed line*) than in Purkinje neurons expressing the non-targeted shRNA (N = 2; n = 11, *black dashed line*). The data in Figure 2F were replotted here to facilitate direct comparison between the effects of the targeted deletion and the acute knockdown of *Scn4b*.

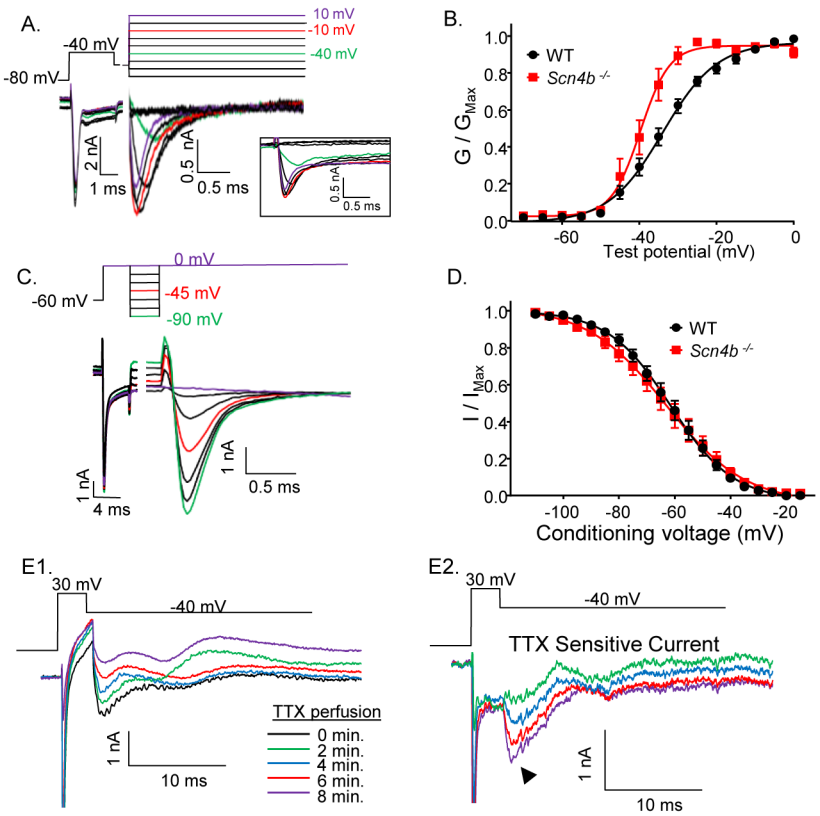

Figure 4. Effects of the targeted deletion of *Scn4b* on Nav currents in adult Purkinje neurons

Representative whole-cell Nav currents recorded from adult WT (*A*) Purkinje neurons in acute cerebellar slices; the voltage-clamp paradigm is illustrated above the records and the currents are shown in the color of the corresponding voltage step. The raw, unsubtracted Nav current records are shown in the boxed inset. The peak amplitudes of the transient Nav currents evoked at each test potential were measured, and peak (transient) Nav conductances were determined and normalized (in the same cell) to the maximal Nav conductance. *B,* Mean ± SEM normalized peak transient Nav conductances in WT (*black*; N = 5; n = 12) and *Scn4b*$^{-/-}$ (*red;* N = 5; n = 13) adult Purkinje neurons plotted as a function of the test potential. *C,* Representative recordings of Nav currents evoked at 0 mV from various conditioning voltages in a WT Purkinje neuron are shown; the voltage-clamp protocol is illustrated above the current records and the currents are shown in the color of the corresponding voltage step. The persistent component of the Nav currents has been digitally subtracted. *D,* The peak transient Nav current amplitudes evoked at 0 mV from each conditioning voltage were measured and normalized to the peak transient Nav current measured after the −120 mV conditioning voltage step (in the same cell). The mean ± SEM normalized peak Nav current amplitudes in WT (*black;* N = 5; n = 15) and *Scn4b*$^{-/-}$ (*red;* N = 3; n = 14) Purkinje neurons were plotted as a function of the conditioning voltage and fitted with first order Boltzmann functions. *E,* Nav currents evoked at −40 mV following a prepulse to +30 mV were also recorded in ACSF with 300 μM $CdCl_2$ and 5 mM TEA before and during perfusion of ACSF containing 1 μM TTX (*E1*). The currents recorded at various times (indicated by different colors) during the perfusion of the TTX-containing bath are

shown and the TTX-sensitive currents were obtained by subtraction of the currents recorded before and after the start of TTX perfusion (*E2*).

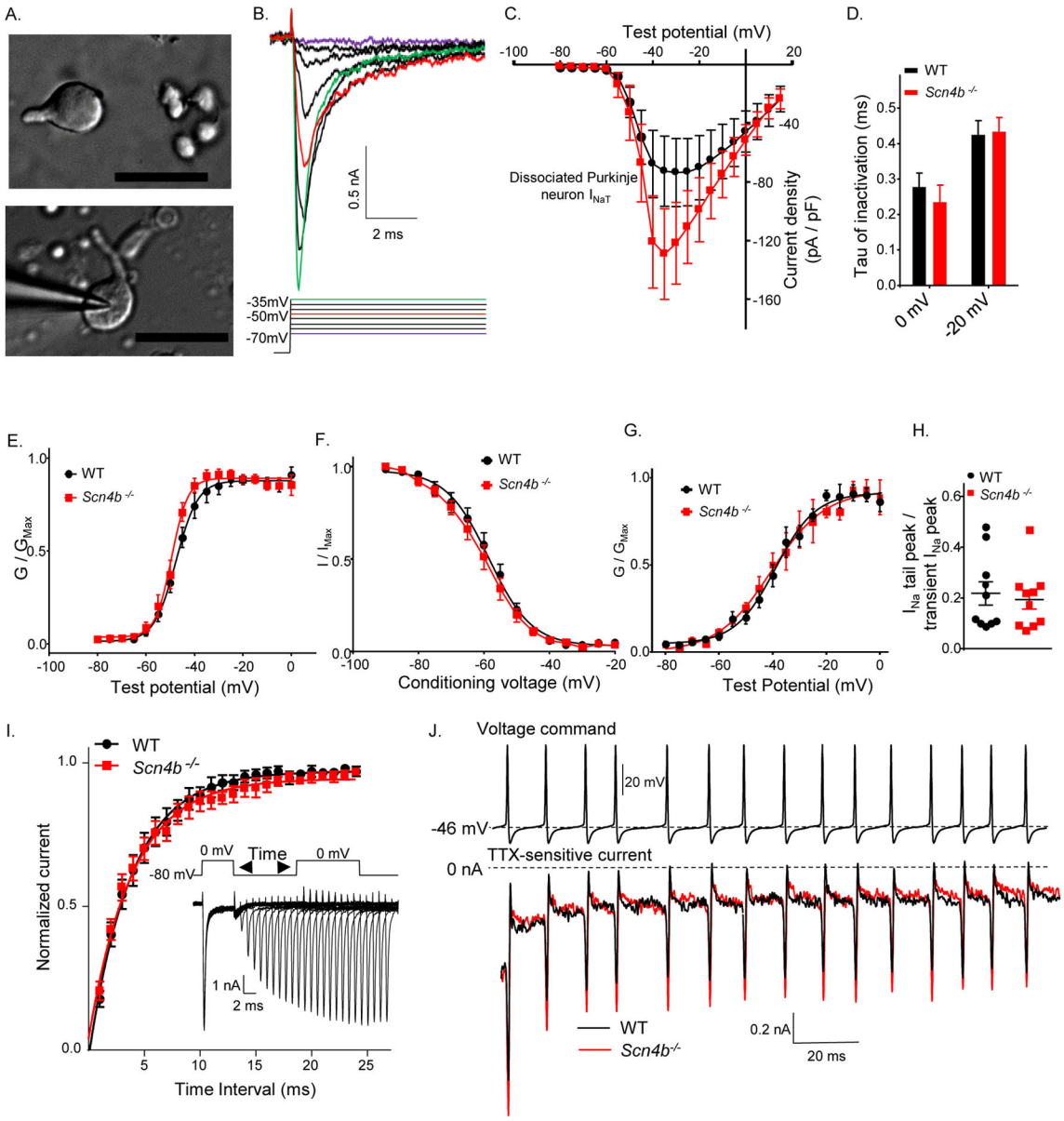

Figure 5. Peak transient Nav current density is higher in acutely isolated neonatal *Scn4b*$^{-/-}$, than in WT, Purkinje neurons

A, Differential interference contrast (DIC) photomicrographs of acutely isolated neonatal cerebellar Purkinje neurons; *scale bars = 50 μm. B,* Representative recordings of whole-cell transient Nav currents evoked at various test potentials; the voltage steps are shown below the current records in the corresponding colors. *C,* The mean ± SEM transient Nav current densities measured in isolated P11–P18 WT (N = 7; n = 12) and *Scn4b*$^{-/-}$ (N = 6; n = 12) Purkinje neurons are plotted as a function of the test potential. See also Figure S2. *D,* The mean ± SEM inactivation tau at 0 mV and −20 mV are similar in WT (N = 7; n = 11) and *Scn4b*$^{-/-}$ (N = 6; n = 12) Purkinje neurons. *E,* Mean ± SEM normalized transient Nav conductances are plotted as a function of test potential. The Boltzmann fits to the data reveal that the voltage-dependences of activation of the transient Nav currents in P11–P18 WT (N

= 7; n = 12) and *Scn4b*$^{-/-}$ (N = 6; n = 13) Purkinje neurons are similar. *F,* The voltage-dependences of inactivation of the transient Nav currents were measured using a protocol as described in Supplemental Experimental Procedures. The Boltzmann fits to the mean ± SEM normalized data reveal that the voltage-dependences of steady-state inactivation in WT (N = 7; n = 10) and *Scn4b*$^{-/-}$ (N = 6; n = 13) Purkinje neurons are similar. *G,* I_{NaP} was measured 10 ms after the onset of the test potential. Boltzmann fits revealed that the voltage-dependences of activation of I_{NaP} are similar in WT (N = 7; n = 12) and *Scn4b*$^{-/-}$ (N = 6; n = 13) Purkinje neurons. *H,* To compare the relative amplitudes of I_{NaP} and I_{NaT} in WT and *Scn4b*$^{-/-}$ Purkinje neurons, the magnitude of the peak Nav tail current, measured at −90 mV following the 0 mV voltage step, was divided by the peak I_{NaT} amplitude in the same cell. *I,* Recovery of Nav currents in WT and *Scn4b*$^{-/-}$ Purkinje neurons from inactivation was measured at 0 mV using the three pulse protocol illustrated; representative Nav currents following each recovery period are shown below. The peak Nav current elicited during the second depolarizing step to 0mV, following each recovery period, was normalized to the peak Nav current measured during the first depolarizing step. Mean ± SEM values were plotted as a function of the time between steps. *J,* Representative action-potential voltage-clamp command waveform (from a holding voltage of −80mV) (*upper*) and TTX-sensitive currents (*below*) recorded in WT (black) and *Scn4b*$^{-/-}$ (red) Purkinje neurons are shown.

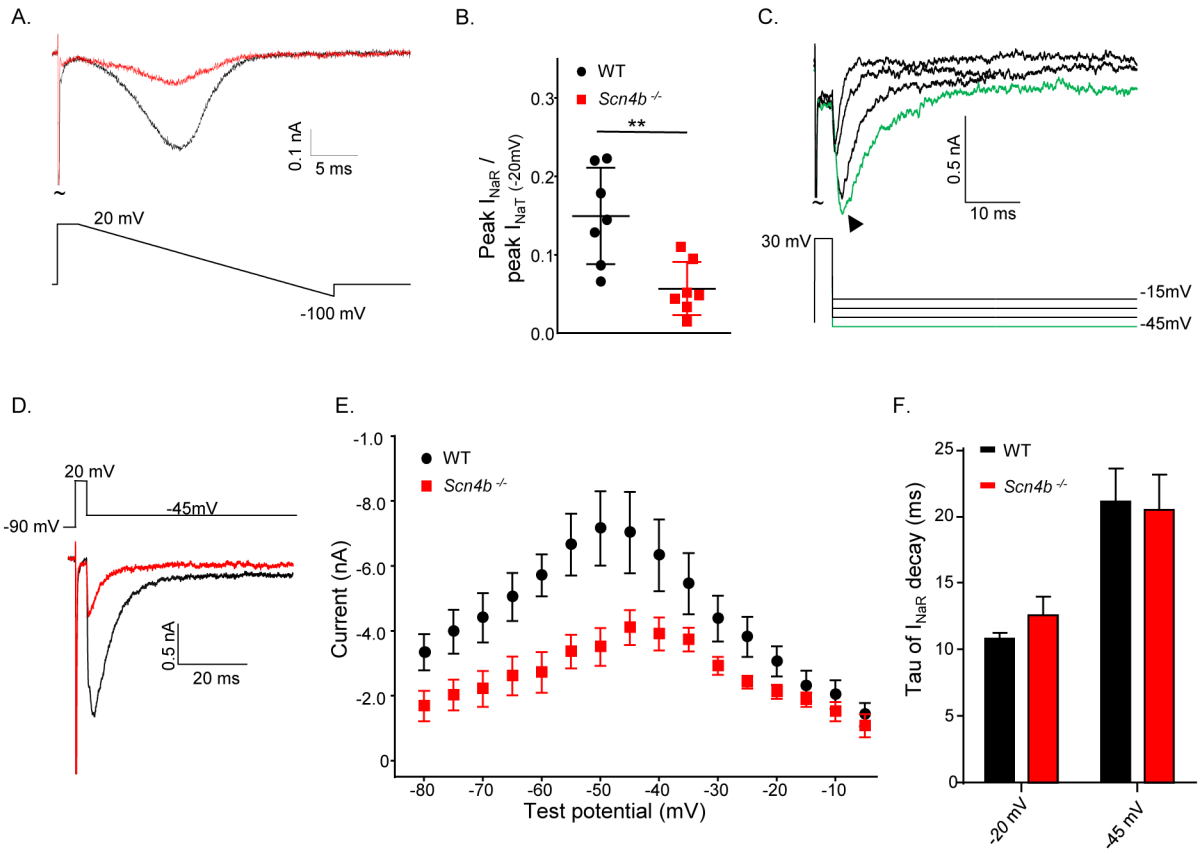

Figure 6. I_{NaR} is attenuated, but not eliminated, in acutely isolated P11–P18 *Scn4b*$^{-/-}$ Purkinje neurons

A, Representative TTX-sensitive Nav currents evoked in low (50 mM) Na^+ bath solution in response to a voltage ramp from +20 to −100 mV (displayed below the current records) in isolated WT (*black*) and *Scn4b*$^{-/-}$ (*red*) Purkinje neurons. *B,* The normalized current values reveal that the TTX-sensitive inward currents were significantly (** $P < .01$, Student's *t*-test) smaller in *Scn4b*$^{-/-}$, than in WT, cells. *C,* Representative TTX-sensitive I_{NaR} recorded at various potentials following depolarizations to +30 mV in a WT Purkinje neuron with 154 mM Na^+ in the bath; the voltage command is displayed below the records and the arrow indicates the peak I_{NaR}. *D,* Representative peak I_{NaR} evoked at −45 mV in isolated WT (*black*) and *Scn4b*$^{-/-}$ Purkinje neurons. *E,* Mean ± SEM peak I_{NaR} in neonatal *Scn4b*$^{-/-}$ (*red;* N = 5; n = 10) Purkinje neurons are significantly (* $P < .05$, two-way ANOVA) attenuated compared with WT (*black*; N = 5; n = 10) Purkinje neurons. I_{NaP}, measured 80 ms into the sweep, was digitally subtracted prior to the analysis. *F,* The time constants (tau) of I_{NaR} decay are similar in neonatal WT (n = 10) and *Scn4b*$^{-/-}$ (n = 10) Purkinje neurons.

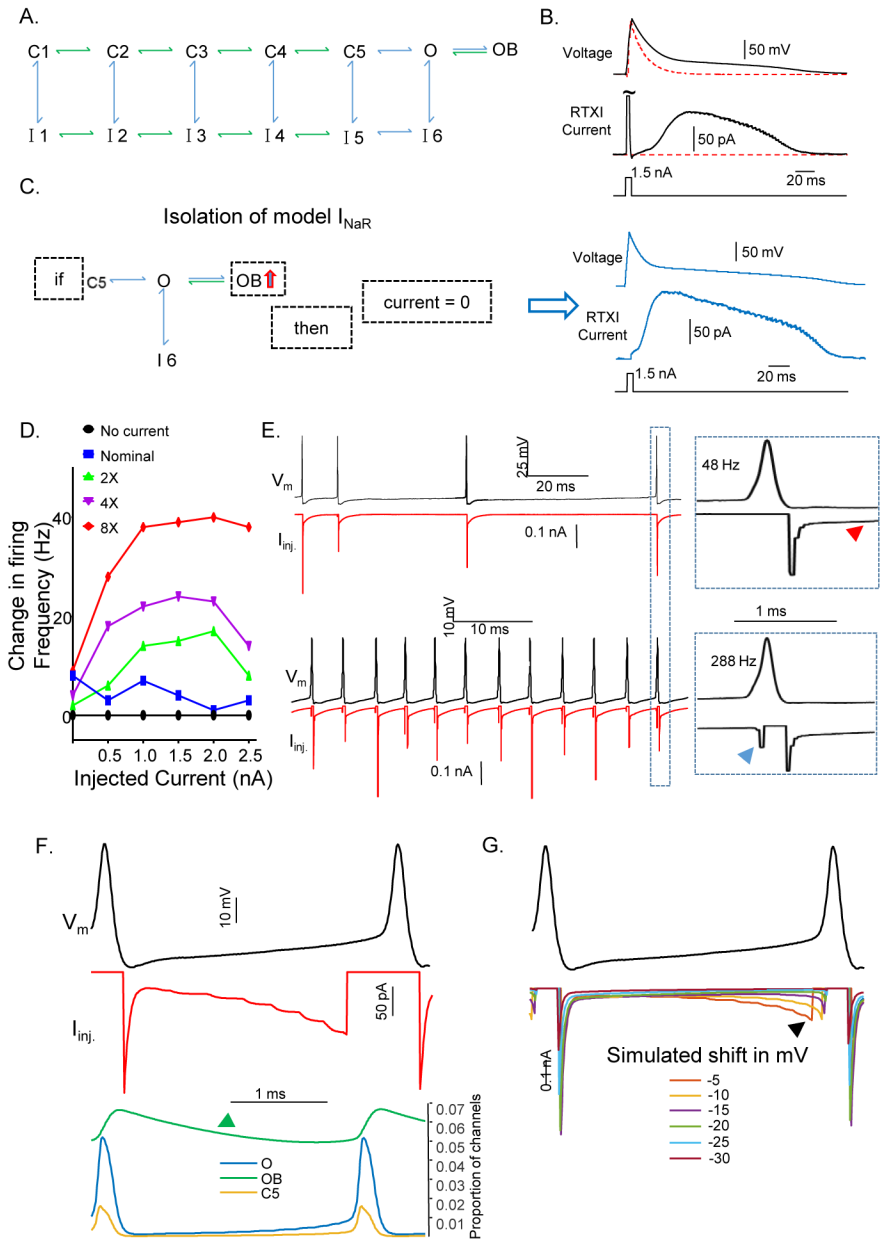

Figure 7. Dynamic clamp-mediated addition of I_{NaR} rescues high frequency firing in *Scn4b*$^{-/-}$ Purkinje neurons

A, Schematic of a thirteen state Markov model describing the transient, persistent and resurgent components of the Nav currents in cerebellar Purkinje neurons (see: Supplemental Experimental Procedures *B,* Brief depolarizing current injections (*bottom traces*) were delivered to a model cell and the resulting change in voltage (*upper trace*), as well as the RTXI current injected (*middle trace*), were measured. The red dashed line reveals the voltage change of the model cell without the addition of I_{Na}. *C, Left-* To isolate and apply the resurgent portion of the I_{Na} model in dynamic clamp, if the proportion of channels in the OB state was increasing, the RTXI current was set to 0. *Right-* With the fast transient portion of the Nav current excluded, the resurgent Nav current was isolated. See also Figure S4. *D,*

Change in the instantaneous firing frequency of a Purkinje neuron in response to 0.0–2.5 nA (x-axis) of depolarizing current with different amounts of modeled I_{NaR} added to the cell via dynamic clamp. *E,* Representative action potentials (*black*) and RTXI currents (*red*) are illustrated. Upper traces show I_{NaR} in a Purkinje neuron firing at 48 Hz, and the lower traces show I_{NaR} in a Purkinje neuron firing at 288 Hz. Boxes (on the *right*) provide increased temporal resolution to display I_{NaR} activation during a single action potential; the red arrow indicates I_{NaR} during the inter-spike interval and the blue arrow indicates I_{NaR} during the upswing of the action potential. *F,* Plots of the changes in the O (*blue*), OB (*green*) and C5 (*yellow*) states as a function of time during action potentials; I_{NaR} is also illustrated (red). The proportion of channels in the OB state (*green arrow*) is decreasing during the inter-spike interval. *G,* Purkinje neuron action potential (*black*) waveforms generated in Matlab with the I_{NaR} model applied. Hyperpolarization of the membrane voltage in 5 mV increments alters the time course of I_{NaR} activation during the inter-spike interval.